

# Design, CFD Simulation, Prototype, and Experimental Investigation of Indirect Active Solar Dryer for Banana

Tigabu Mekonnen Belay, Samson Mekbib Atnav



**Abstract:** Indirect active tray solar dryer was designed, CFD simulated, and constructed for the drying of banana in Addis Ababa, Ethiopia. The experimental investigation was done after the CFD ANSYS Fluent simulation of different parameters based on the uniformity temperature and air flow distributions on the symmetry plane. The performance of the designed solar dryer was compared with that of the open sun dryer method, based on drying rate, moisture ratio, and moisture content on a wet and dry basis. From fourteen different mathematical drying thin layer kinetics models, the maximum correlation coefficient of 0.999574, the minimum root mean square of 0.0001352, and the minimum reduced chi-square of 0.007353 were obtained for the Verma et al. model for the slice banana in the designed active solar dryer. Recycling the air from the outlet of the drying chamber on the first day is not possible because the quality of the air is lower when compared with ambient air. The outlet air temperature and relative humidity of the drying chamber were 4.39°C higher and 8.24% lower than the ambient air temperature and relative humidity respectively, so it is possible to recycle the air after the first day. The average moisture content removed from the product in the designed solar dryer and open sun dryer was 68.01% and 51.01%, respectively, in the 22 and half5 drying hour. The difference between the maximum and minimum moisture removal was 4.47%. It indicates there is a uniform drying in the designed solar dryer. The overall solar air collector efficiency was 33.80% and the maximum drying efficiency was 31.10 %.

**Key Word;** Open sun dryer; CFD simulations; Mathematical drying model; Moisture content; Performance; Solar drying; Uniformity in drying

## I. INTRODUCTION

One of the oldest uses of solar energy is for drying by exposing the product to the sun. It has been used since the dawn of mankind mainly for different applications like food preservation for winter and other applications like drying of cloth, construction material like soil brick for their home, and animal skin for dressing.

From this prehistoric time on, mankind has used solar radiation as the only source of thermal energy [1]. A low-cost active, indirect, environmentally friendly solar dryer was designed for different agricultural products. The solar convection drying system is used to preserve fruits, vegetables, grains, fish, meat, wood, and other agricultural products, which are free and renewable sources of energy [2, 3]. An active solar dryer is more suitable for the drying of higher moisture contents [4]. Bananas are one of the important fruits grown around the world that are members of the Musaceae, genus Musa family [5]. Banana contains potassium, vitamin B6, vitamin C, and various antioxidants and phytonutrient, and the banana peel (BP), contains Iron, cadmium, chromium, Nickel, Copper, Lead, and Zinc conducting materials. Due to its importance, banana is grown as a second main fruit in 120 countries. The world's production of bananas is 86 million ton [5]. According to FDRE CSA Agricultural Survey Data of the average of three years of (2010, 2012, and 2013EC) report on area and production of major crops, more than 10,134,318.25 quintals of fruit crops were produced from 125,725.75 hectares of land under fruit crop production. According to the report, banana contribute the most in terms of production area and volume. Bananas account for 58.06 percent of the average amount used for fruit cultivation, followed by avocados, which account for 18.06 percent. Bananas, mangoes, avocados, papayas, and oranges accounted for 63.58%, 12.22%, 13.38%, 6.07%, and 3.42% of total fruit production, respectively. For the experimental investigation, banana was used to study its drying characteristics since it has good nutrients when dried [6]. The moisture content and maximum allowable temperature of different agricultural products were presented [7, 8]. The efficient performance of a solar dryer is mainly depending on the good distribution of the thermal and flow fluid inside the dryer body [9]. CFD simulation was able to simulate and predict the temperature and air flow distribution inside the developed industrial-scale solar dryer for various possible operating conditions without the need to run a physical experiment, which is time-consuming, tedious, and expensive [10]. There is a good agreement between the simulated and experimental data [11]. In different research studies, CFD simulation was used for their study of solar dryers [12- 16]. There are different tray arrangements used by different researchers [9, 11, 17- 25]. This paper aims to increase the uniformity of drying by studying the different paramerts effects of different tray arrangements as shown in Figure 1

Manuscript received on 23 June 2022 | Revised Manuscript received on 05 July 2023 | Manuscript Accepted on 15 August 2023 | Manuscript published on 30 August 2023.

\*Correspondence Author(s)

Tigabu Mekonnen Belay\*, Department of Mechanical Engineering, Addis Ababa Science and Technology University, Ethiopia. E-mail: [tigabumekonnenb@gmail.com](mailto:tigabumekonnenb@gmail.com), ORCID ID: [0000-0003-0596-1276](https://orcid.org/0000-0003-0596-1276)

Samson Mekbib Atnav, Department of Mechanical Engineering, Addis Ababa Science and Technology University, Ethiopia. E-mail: [samson\\_mekbib@aastu.edu.et](mailto:samson_mekbib@aastu.edu.et), ORCID ID: [0000-0002-1220-6722](https://orcid.org/0000-0002-1220-6722)

© The Authors. Published by Lattice Science Publication (LSP). This is an open access article under the CC-BY-NC-ND license (<http://creativecommons.org/licenses/by-nc-nd/4.0/>)

(a) 2D and (b) 3D and the effect of increasing the length and effect of increasing the height of drying chamber in Figure 2 (A) and (B) respectively using CFD simulations of Ansys Fluent. Finally based on the CFD simulation of air flow and temperature distributions uniformity in the symmetry plane of the drying chamber experimental test was done to improve the uniformity of product in the designed active solar dryer. In this paper an active solar dryer for drying banana designed, CFD simulated using Ansys Fluent Software, conduct experiments on the prototype of the designed active solar dryer, and choose the best fitting drying kinetics model for drying banana using the active solar dryer.

## II. MATERIALS AND METHODS

### A. CFD Simulations

In this CFD simulation Ansys fluent software R19.2 has been utilized to analyze the uniformity of air flow and temperature distributions of the assigned five different tray arrangements and four different drying chamber at different length and four drying chamber at different height for selected tray arrangements at inlet velocity of 0.83m/s, at a fixed inlet temperature of 323.15K, within adiabatic outer wall and internal wall convective heat transfer at temperature of 293.15K and convective heat transfer coefficient of 2.5w/m.K. The 3D for both drying chambers, sampled banana and frame was done using solid work and saved in IGES extensions. The designed geometry edited using Ansys design modulars.

The cover glazing of the SAC was made from float glass of 4 mm in thickness. The wall of the solar air collectors and drying chamber was made up of plywood with a thickness of 18 mm. Plywood is used to construct the wall of solar air collector and drying chamber because it was easily available, low cost, and insulated (to prevent heat loss) in Ethiopia. The black painted aluminum sheet with a thickness of 1mm and a dimension of 500 mm × 1000 mm was used as a solar absorber plate. As glazing or cover, transparent window glass with a thickness of 4mm, transmittance of 0.87 and dimensions of 522 mm × 1022 mm were used. All the supports and the wall of the solar air collector and drying chamber were painted black to decrease the change in temperature of the insides and outsides of both the solar air collector and drying chamber. The edge of the plywood for the wall of the solar air collector and drying chamber was cut in an L shape for proper fit. The gap between the solar air heater and the cover glass is 9 cm. The tray was constructed with wire mesh and a plywood frame. The assembly of the system was done using thin nails and linking components like glue and wood fix cola. There was plastic to cover the solar drying system at night and on rainy days. It is used to prevent the entrance of rain during rainy days to the drying chamber and solar air collector. It was also used to protect the cabinet from the absorption of moisture from the environment. A stainless-steel cutter blade was used to slice the banana into the desired thickness and cylindrical shape. As much as possible, the diameter and thickness of the slice must be

equal. A computer cooling fan of DC 12V, 0.24A Foxconn Brushless Fan model PVA092G12M was used to force the air to pass over the absorber plate. Fans were powered by utility electricity since it was fully available at the performance testing or working area. The banana sample of average diameter of 3.5cm diameter with distance between the sliced banana of 4cm, and thickness of 5mm was used. The bulk density of banana in this study is 1.14g/cm<sup>3</sup> based on the data on (FAO). The fluid domain is equal to the volume of the drying chamber except the sample of banana and frame subtract. The net area of each tray is equal that was 0.6m<sup>2</sup>. The inlet and outlet diameter of both the solar air collector and drying chamber was 7.5cm. A double precision solver and tetrahedral cells are included in each sketch. The set-up section was done using double precision and parallel solver of three processor. The solver is pressure-based, absolute velocity formulations, steady and gravity-based. Outlet: assuming the gauge pressure is zero. Even though the simulation was done in three dimensions, the analysis was carried out on the symmetry plane [26]. Velocity inlet and pressure outlet was considered on the CFD analysis of drying chamber [27]. The RNG k-ε turbulence model with enhanced wall function is used to solve the transport equations for turbulent flow and energy dissipation rate. On the interface of solid and fluid there is no slip conditions. The equations of flow and heat transfer are solved for the fluid zone using air properties. The different tray arrangement with tetrahedral mesh type, quality of mesh with skewness of 0.4 used, quadratic element type, and element size of 0.003m. For terminating solution in ANSYS fluent residual value for energy that is 10<sup>-6</sup> and 10<sup>-3</sup> for all other equations used. The properties of the air was as follow thermal conductivity of 0.02588w/m.K, density of 1.164kg/m<sup>3</sup>, specific heat capacity of 1007J/kg.K, and dynamic viscosity of 1.878\*10<sup>-5</sup>kg/m.s [28]. The thermal conductivity and diffusivity values of green and yellow bananas changed from 0.302 to 0.338 W/m.K and 1.442 × 10<sup>-7</sup> to 1.5 × 10<sup>-7</sup> m<sup>2</sup>/s respectively [29].

**Tray arrangement:** The 2D and 3D tray arrangements are shown in the Figure 1 (a) and (b) respectively. The Table 1, show the details of the tray including the size, vertical space, numbers of trays, number of columns and rows, and area of each tray arrangements studied in this paper. A rectangular drying chamber with internal dimensions of 50cm × 50cm × 50cm used for CFD Simulations to identify the proper tray arrangements. The positions of the inlet and outlet for five drying chambers were also the same. The diameter of the inlet and outlet of the drying chamber were 7.5cm, and the center of the inlet and outlet were equal from the bottom and top wall respectively. In all cases, the bottom tray is placed above 12.5 cm from the drying chamber wall, and the upper tray is placed 12.5 cm below the drying chamber's upper wall. Table 2, displays the average and maximum skewness as well as the number of elements for each of the five drying chambers, including the dried banana sample.

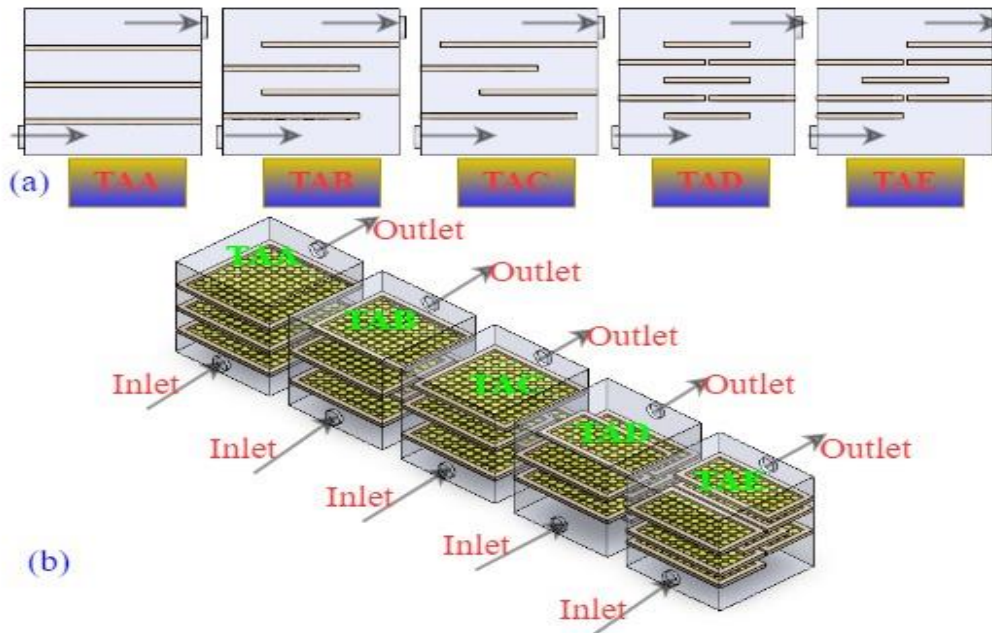


Figure 1: 2D (a), and 3D (b) of five different tray arrangement

The flow of the air is perpendicular, tangent or over the product to be dried since the flow of the air depends on the tray arrangements. For tray arrangements placed zig zag, the flow of the air between the trays is zig zag. As shown in the Figure 1, the size of the drying chamber, the positions of the inlet and outlet are equal and similar. In Figure 1, the only difference is the arrangements of trays.

Table 1: Details of the five different tray arrangements

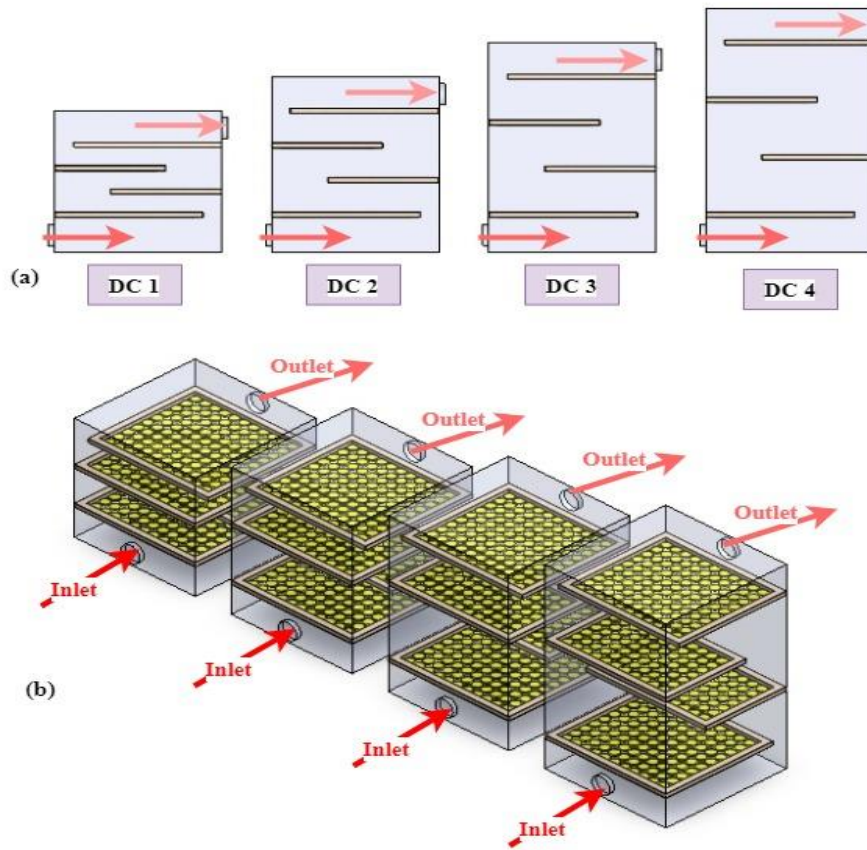
Tray Arrangement	Number of trays	Number of column	Vertical space	Length (cm)	Width (cm)
TA-A	3	1	12	44.72	44.72
TA-B	4	2	7.83	33.54	44.72
TA-C	2	1	7.83	39.14	44.72
	2	1	7.83	27.95	44.72
TA-D	7	3	5.75	19.167	44.72
TA-E	7	3	5.75	19.167	44.72

Table 2: The number of tetrahedral cells for four different solar air collectors

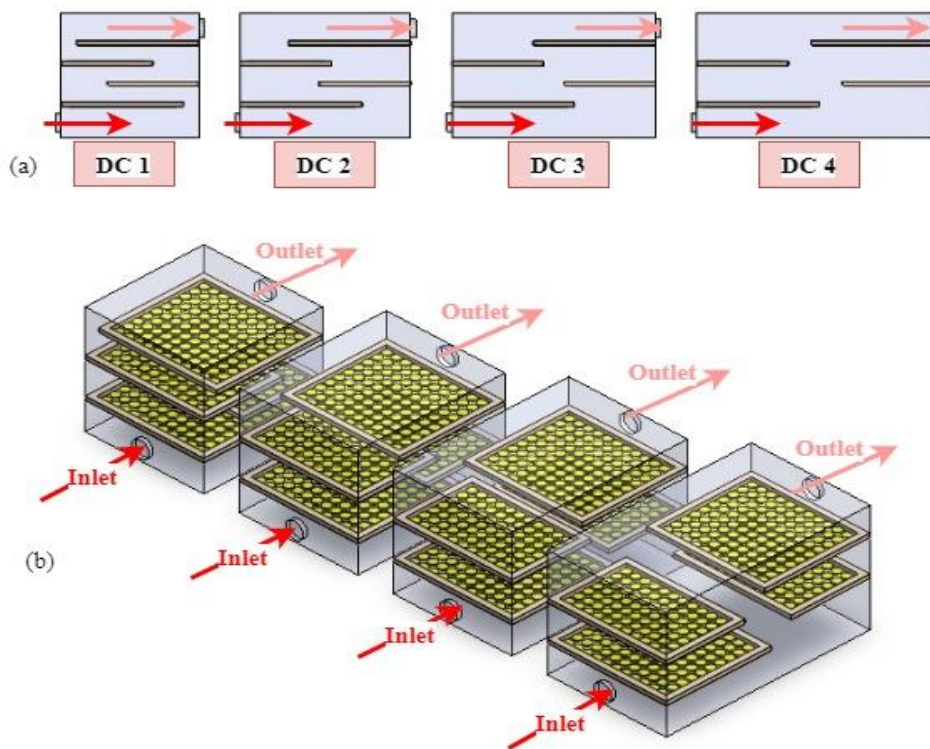
Sket-ch	Tetrahedral cell	Number of nodes	Mesh metric			
			Min	Max	Aver	SD
TAA	2866775	4054579	3.9631e-4	0.93624	0.2493	0.10144
TAB	2913306	4121115	2.118e-4	0.95208	0.25204	0.10347
TAC	2955485	4176984	3.1196e-4	0.96593	0.25103	0.10228
TAD	3054403	4332297	2.7327e-4	0.93902	0.25241	0.10346
TAE	3060374	4338463	4.1976e-4	0.93902	0.25153	0.10342

**Effect of increasing the height and length of the drying chamber:** Following the selection of the best TA based on the CFD simulation results, the effect of drying chamber height in four drying chambers was compared with an equal width and length of drying chamber with a 50 cm and a height of 50 cm, 62 cm, 74 cm, and 86 cm. The vertical space between consecutive trays is 7.67cm, 11.67cm, 15.67cm, and 19.67cm for a height of the drying chamber of 50cm, DC 1, 62cm, DC 2, 74cm, DC 3, and 86cm, DC 4, respectively. The schematic of the four different drying chambers for selected tray arrangements was presented in 2D and 3D in Figure 2 (A). This is another study on the effect of increasing the length of the drying chamber using CFD simulation analysis. When the length of the drying chamber increases, the front

wall's side stacks become far apart from the end rear wall. Similarly, the tray stacked on the rear wall becomes far apart from the front wall. The four-drying chamber with selected TA of equal width and height of 50 cm and with different lengths of 50 cm, 62 cm, 74 cm, and 86 cm, as shown in the Figure 2 (B) was considered for the CFD simulation analysis.



(A) Effect of increasing the height DC



(B) Effect of increasing the length of DC

Figure 2: The effect of increasing height and length of drying chambers (a) 2D, (b) 3D

The details of the tetrahedral cell for different drying chambers with different height are presented in Table 3.

**Table 4: The number of tetrahedral cells for four DC with different height**

Height of DC	Tetrahedral cell	Number of nodes	Mesh metric			
			Min	Max	aver	StDv
50cm	10021995	14025941	3.476e-4	0.9378	0.244	0.1003
62cm	11388270	15908658	2.6268e-4	0.9378	0.2430	0.1003
74cm	13308879	18528781	1.1404e-4	0.9378	0.2424	0.1001
86cm	14882500	20682743	2.6546e-4	0.9378	0.2414	0.1000

**CFD Simulation for the effect of increasing the length of DC** Table 5 presents the tetrahedral cell, number of nodes, and mesh metrics of each drying chamber at different length.

**Table 5: The number of tetrahedral cells for four DC with different length**

Length of DC	Tetrahedral cell	Number of nodes	Mesh metric			
			Min	Max	Aver	StDv
50cm	10021995	14025941	3.476e-4	0.9378	0.2440	0.1003
62cm	11361454	15870529	3.0827e-4	0.9378	0.2438	0.1004
74cm	13129737	18289226	3.6444e-4	0.9378	0.2425	0.1002
86cm	14046676	19565787	1.8990e-4	0.9378	0.2419	0.1003

**B. Experimental Test**

The experimental investigation of the indirect active solar dryer was done after the CFD simulation of tray arrangements and the effect of increasing the length of the drying chamber. The experimental investigations were conducted near the college of electrical and mechanical engineering, AASTU, Addis Ababa, Ethiopia at a latitude of 8.883 and a longitude of 38.8103 degrees in the month of June.

There are two solar air collectors having equal dimensions in Figure 4, solar air collector one (SAC 1) and solar air collector two (SAC 2). The first solar air collector has two inlets at the ends of both the left and right sides and an outlet at the center. The two-fan unit is installed at the inlet of the first solar air collector. The air from the first solar air collector outlet enters the second solar air collector via the flexible duct near to the corner, and the air, after getting energy from the second solar air collector, leaves at the corner and enters the drying chamber of the center.

**Instrumentations:** There are different instruments that are used to measure and record the data. A temperature and relative humidity sensor with uncertainty of  $\pm 0.5^\circ\text{C}$  and  $\pm 1\%$  respectively, and the uncertainty for pyranometer and digital sensitive weight balance was  $\pm 5\text{w/m}^2$  and  $\pm 0.01\text{g}$  respectively.

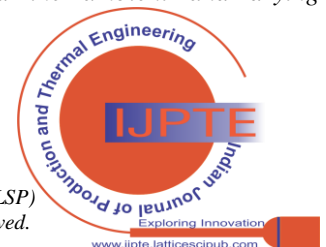
**Unloading test:** During the unloading test, the uncertainty of different measuring devices, sensors, solar air collectors one and two, flexible duct, and drying chamber was checked. The sensor used for measuring the air property was mounted at the solar air collector one outlet, solar air collector two inlets, at the middle of the solar air collector two outlets, drying chamber inlet connecting flexible duct, inside the drying chamber and at the outlet of the drying chamber. The pyranometer was placed at a similar tilt angle to the solar air collector.

**Loading Test:** The loading conditions experiment was done for a total of four days when there was sunlight. The banana fruit was obtained from the local super market in Addis

Ababa. Before the experiment, the average diameter of the banana was checked for an average diameter of between 3 cm and 4 cm, peeled, and the two ends removed by knife, and sliced to a thickness of 5 mm with a stacked blade on MDF wood. To check the moisture content, five samples were taken from each tray. During the measuring of the mass of the sampled banana, all the fans will stop, and the open sun dryer is prohibited from getting solar radiation because of its effect on the performance comparisons of the active indirect solar dryer and the open sun dryer. The system was worked for 30 minutes before data recording started by closing the outlet of the solar air collector for 15 minutes, and then opening and waiting another 15 minutes for preheating of the system as a whole, since at the initial there is some temperature decrease due to the temperature inside the duct, solar air collector, and drying chamber, and also the supplied air starts to heat the surface of the flexible duct, solar air collector, and drying chamber. The mass or amount of banana slices to be placed is then obtained and placed on the tray in a thin layer. In all cases of product distribution, the distribution is similar, as the space between slice and arrangement is uniform in all cases. To place the banana uniformly based on the load density of  $2.5 \text{ kg/m}^2$ , the total mass of the banana in each tray was calculated by multiplying the load density by the area of the tray.

During the drying process,

- ✓ Register the solar radiation at a similar tilt angle to the solar air collectors.
- ✓ Register the temperature, and relative humidity at the outlet of solar air collector one, the inlet of solar air collector two, between solar air collector two outlet and the drying chamber inlet, inside the drying chamber and the ambient and drying chamber outlet.



**Design, CFD Simulation, Prototype, and Experimental Investigation of Indirect Active Solar Dryer for Banana**

- ✓ Remove the sample product after the drying time of the day of drying to measure the mass.
  - ✓ Measure the total mass of the five-sample bananas in each tray.
  - ✓ Places the sample on tight plastic and return to the drying chamber in the morning.
- When the sample in the dryer reached the desired moisture level, the drying process was terminated.

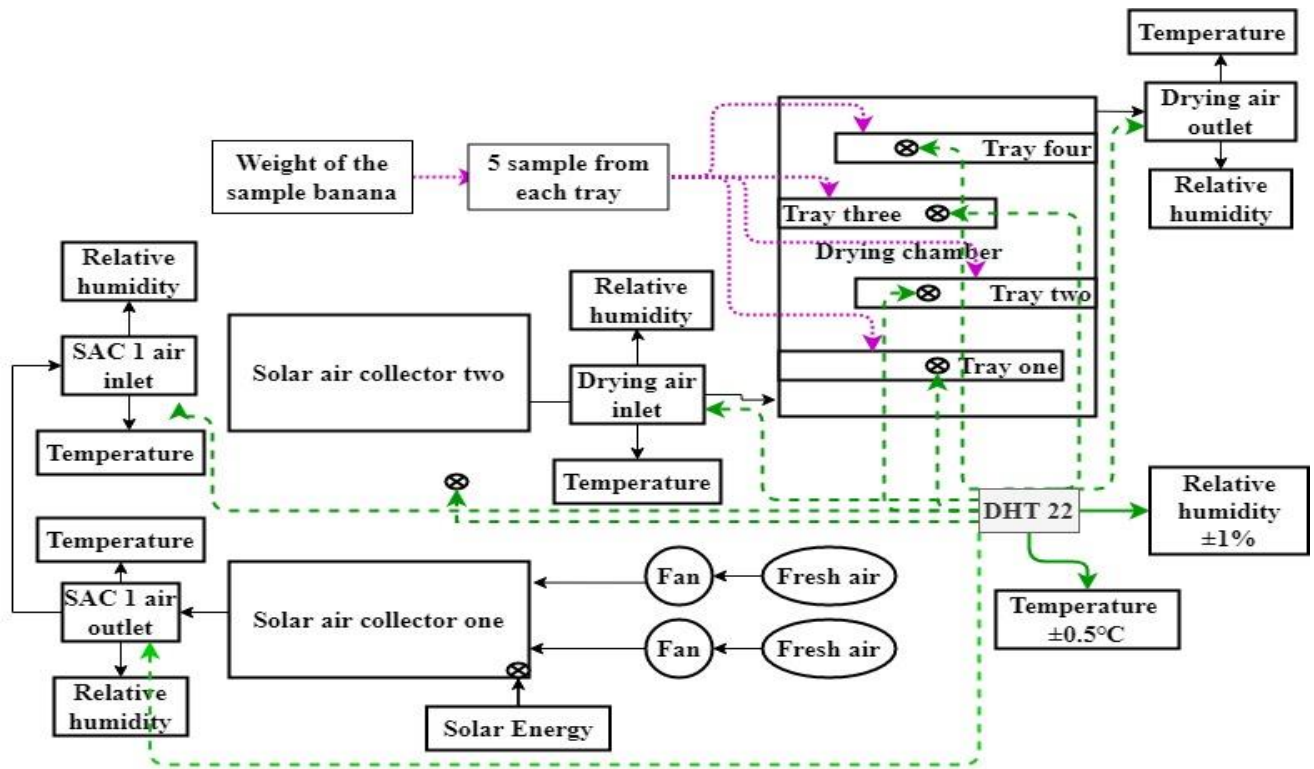
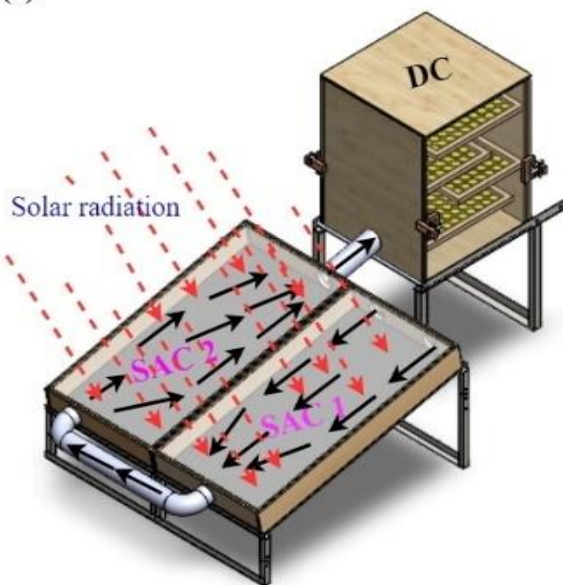


**Figure 3: Flow diagram of thin layer active solar drying process and measuring**

(a)



(b)



**Figure 4: Schematic (a) and experimental (b) picture of the designed solar dryer.**

**Open sun dryer:** In the open sun dryer, the amount of the banana dried was based on the load density of  $2.5\text{kg/m}^2$ , with a thickness of 5mm, and the same distribution of the banana slices on the wire mesh as the one inside the drying chamber. The tray with wire mesh and frame similar to the tray used inside the drying chamber was used and placed above 10 cm from the ground on the concrete at the end of the tray as a holder.

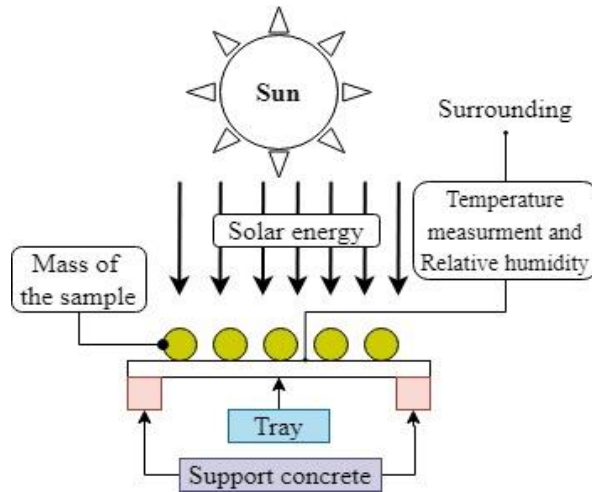


Figure 5: Flow diagram of thin layer of open sun drying process

### III. UNCERTAINTY AND PERFORMANCE EVALUATIONS

#### A. Uncertainty Evaluations

The air temperature, air relative humidity, solar radiation, and sample weight were measured in this experimental test. There are errors and uncertainties due to the design of the experiments, inaccurate reading of instruments, calibration, and instrument resolution. The overall uncertainty of a measurement is the root-sum-square combination of the uncertainties of all the subordinate measurements considered to be part of the present measurement. This is the uncertainty due to errors introduced by changing environmental conditions such as temperature and humidity. For further total uncertainty analysis of the instrument used to measure temperature, pressure, velocity, relative humidity, and mass is sum the square of the uncertainty of the instrument,

connection, reading, and other of the instrument itself and take the square root of the summation [30].

$$U_{OA} = \sqrt{U_{BE}^2 + U_{RE}^2 + U_{OE}^2 + U_{EE}^2} \quad (1)$$

Uncertainty due to repeatability or random error ( $U_{RE}$ ) is determined from the standard deviation of the sample data.

$$\sigma = U_{RE} = \sqrt{\frac{\sum_{i=1}^N (x_i - \bar{x})^2}{N - 1}} \quad (2)$$

Where;  $\sigma$  is standard deviations,  $N$  is number of data measurements,  $\bar{x}$  is the average of the measurements.

The uncertainty due to systematic error for uniformly distributed error ( $U_{BE}$ ) is given by [31]:

$$U_{BE} = \frac{L}{\sqrt{3}} \quad (3)$$

Where  $\pm L$  are the containment limits which may be taken from manufacturer tolerance.

Table 6: Instruments Manufacturing tolerance limit value

Parameter	Instrument	Brand and model	Accuracy
Temperature	DHT-22	Thermistor	$\pm 0.5^\circ\text{C}$
Humidity	DHT-22	Capacitor	$\pm 1\%$
Solar radiations	Pyranometer	Apogee; Model: SP - 101; Non-linearity: $< 1\%$ (up to 1750 W/m <sup>2</sup> )	$\pm 4.5\text{W/m}^2$
Weight of sample	Digital sensitive weighting	K. Roy: Model: DJ 602A	$\pm 0.01\text{g}$

Table 7: The uncertainty measured in the experiment

Parameter measured	unit	$U_{BE}$	$U_{RE}$	$U_{OE}$	$U_{EE}$	$U_{OA}$
Air temperature	$^\circ\text{C}$	$\pm 0.289$	$\pm 0.36$	$\pm 0$	$\pm 0$	$\pm 0.462$
Air relative humidity	%	$\pm 0.577$	$\pm 0.22$	$\pm 0$	$\pm 0.5$	$\pm 0.795$
Mass of sample	g	$\pm 0.006$	$\pm 0$	$\pm 0.001$	$\pm 0.007$	$\pm 0.009$
Solar radiations	$\text{W/m}^2$	$\pm 2.60$	$\pm 0$	$\pm 1.5$	$\pm 2.5$	$\pm 3.906$

The result obtained in the uncertainty analysis indicates that the measured data is accurate enough to assess the performance of the designed active solar dryer. Total uncertainty in the solar air collector estimation due to solar air collector one temperature ( $T_{in}$ ), solar air collector two outlet temperature ( $T_{out}$ ) and solar radiations ( $I$ ) using equation (4) [31, 32].

$$\eta_{SCU} = \sqrt{\left(\frac{\partial \eta_{SC}}{\partial T_{out}}\right)^2 (U_{OA}, T_{out})^2 + \left(\frac{\partial \eta_{SC}}{\partial T_{in}}\right)^2 (U_{OA}, T_{in})^2 + \left(\frac{\partial \eta_{SC}}{\partial I}\right)^2 (U_{OA}, I)^2} \quad (4)$$

Where,  $\eta_{SCU}$  is the overall uncertainty solar air collector efficiency,  $\eta_{SC}$  is the solar air collector efficiency. The properties of the air were as follow thermal conductivity of  $0.02588\text{W/m.K}$ , density of  $1.164\text{kg/m}^3$ , specific heat capacity of  $1007\text{J/kg.K}$ , and dynamic viscosity of  $1.878 \times 10^{-5}\text{kg/m.s}$  [28].

$$R_e = \frac{\rho \times V \times D}{\mu} \quad (5)$$

Where;  $R_e$  is Reynolds number;  $\rho$  is density,  $V$  inlet velocity,  $D$  inlet diameter,  $\mu$  is dynamic viscosity. By substituting all the known parameters, the Reynold number becomes which is greater than 2300. That means the flow is turbulent flow

**B. Performance Evaluations**

**Drying rate:** The drying rate DR can be calculated as follow using rate methods [34].

$$DR = \frac{dM}{dt} = \frac{M_{t+\Delta t} - M_t}{\Delta t} \quad (6)$$

here;  $DR$  is drying rate,  $M_{t+\Delta t}$  the mas of the product measure at time  $(t + \Delta t)$ ,  $M_t$  is the mass of the product at initial time.

**Mositure ratio:** The moisture ratio of the dried product can be measured using the fromula from [35], the moisture ratio is used for the comparisions of the performnace of solar dryer simply by measuring the mass of the dried product before and after drying using weight balance.

$$MR = \frac{M_t - M_{eq}}{M_i - M_{eq}} \quad (7)$$

Since  $M_{eq} \ll M_i$  so, the moisture ratio will simplified as the sollow

$$MR = \frac{M_t}{M_i}$$

Where;  $MR$  is moisture ratio,  $M_t$  is instantaneous moisture content,  $M_i$  is initial moisture content, and  $M_{eq}$  is equilibrium moisture content.

**Moisture contentn in dry and wet basis:** Moisture content (%) wet basis [8, 36]

$$MC_{wb} = \frac{M_{wet} - M_{dry}}{M_{wet}} \times 100 \quad (8)$$

Moisture content (%) in dry basis

$$MC_{db} = \frac{M_{wet} - M_{dry}}{M_{dry}} \times 100 \quad (9)$$

**Table 8: Mathematical model applied to the solar drying curves**

Modeling	Equations
Lewis	$MR = \exp(-kt)$
Page	$MR = \exp(-kt^n)$
Modified page	$MR = \exp(-(kt)^n)$
Henderson and Pabis	$MR = a. \exp(-kt)$
Logarithmic	$MR = a. \exp(-kt) + c$
Two terms	$MR = a. \exp(-k_0t) + b. \exp(-k_1t)$
Wang and Singh	$MR = 1 + at + bt^2$
Verma et al	$MR = a. \exp(-kt) + (1 - a). \exp(-gt)$
Midilli and Kucuk	$MR = a. \exp(-kt^n) + bt$
Diffusion approach	$MR = a. \exp(-kt) + (1 - a). \exp(-kbt)$
Two term exponentials	$MR = a. \exp(-kt) + (1 - a). \exp(-kat)$
Simplified Fick's diffusion	$MR = a. \exp(-c(t/L^2))$
Modified Page equation -2	$MR = \exp(-k(t/L^2)^n)$
Approximation of diffusions	$MR = a. \exp(-kt) + (1 - a)(-kbt)$

Where;  $M_{wet}$  is initial weight of the sample,  $M_{dry}$  is final weight of the sample,  $MC_{wb}$  is moisture content in wet basis, and  $MC_{db}$  is moisture content in dry basis

**C. Mathematical Drying Kinetics modeling**

A non linear regration analysis study was caried out to select the appropriate models for banana and peach drying, the two parameters of coefficient of determinations  $R^2$  and chi-

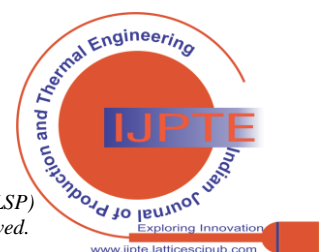
squared coefficient  $x^2$  is used, the fit is based on higher value of  $R^2$  and lower value of  $x^2$  [35]. The coefficient of determination (R), reduced chi-square ( $x^2$ ) [37, 38], and root mean square error (RMSE) [38] between observed and anticipated moisture ratios are used to compare different mathematical models [30]. Different thin layer mathematical modelin were used by different researchers [19, 30, 39-44].

$$R^2 = \frac{\sum_{i=1}^{i=N} ((MR_{exp,i} - MR_{exp,m})^2 - (MR_{prd,i} - MR_{exp,i})^2)}{\sum_{i=1}^{i=N} ((MR_{exp,i} - MR_{exp,m}))} \quad (10)$$

$$x^2 = \frac{\sum_{i=1}^{i=N} (MR_{exp,i} - MR_{predicted,i})^2}{N - n} \quad (11)$$

Where:  $MR_{exp,i}$  = ith experimental value moisture ratio,  $MR_{pred,i}$  = ith predicted value of moisture ratio,

$MR_{exp,m}$  = mean experimental moisture ratio,  $N$  = Number of measurements,  $n$  = Number of model's constant



IV. RESULT AND DISCUSSION

A. CFD Simulations

The most suitable feasible assessment was assessed by comparing the temperature and air flow distributions on the symmetry plane of the drying chamber. The temperature distribution profiles are shown in Figure 6. Based on the

obtained results, the arrangement of trays on the solar dryer has a more significant effect on the temperature and air flow distribution inside the drying chamber. The temperature of the air decreases from the bottom to the top due to heat loss due to convective heat transfer on the assumed wall of the sample banana.

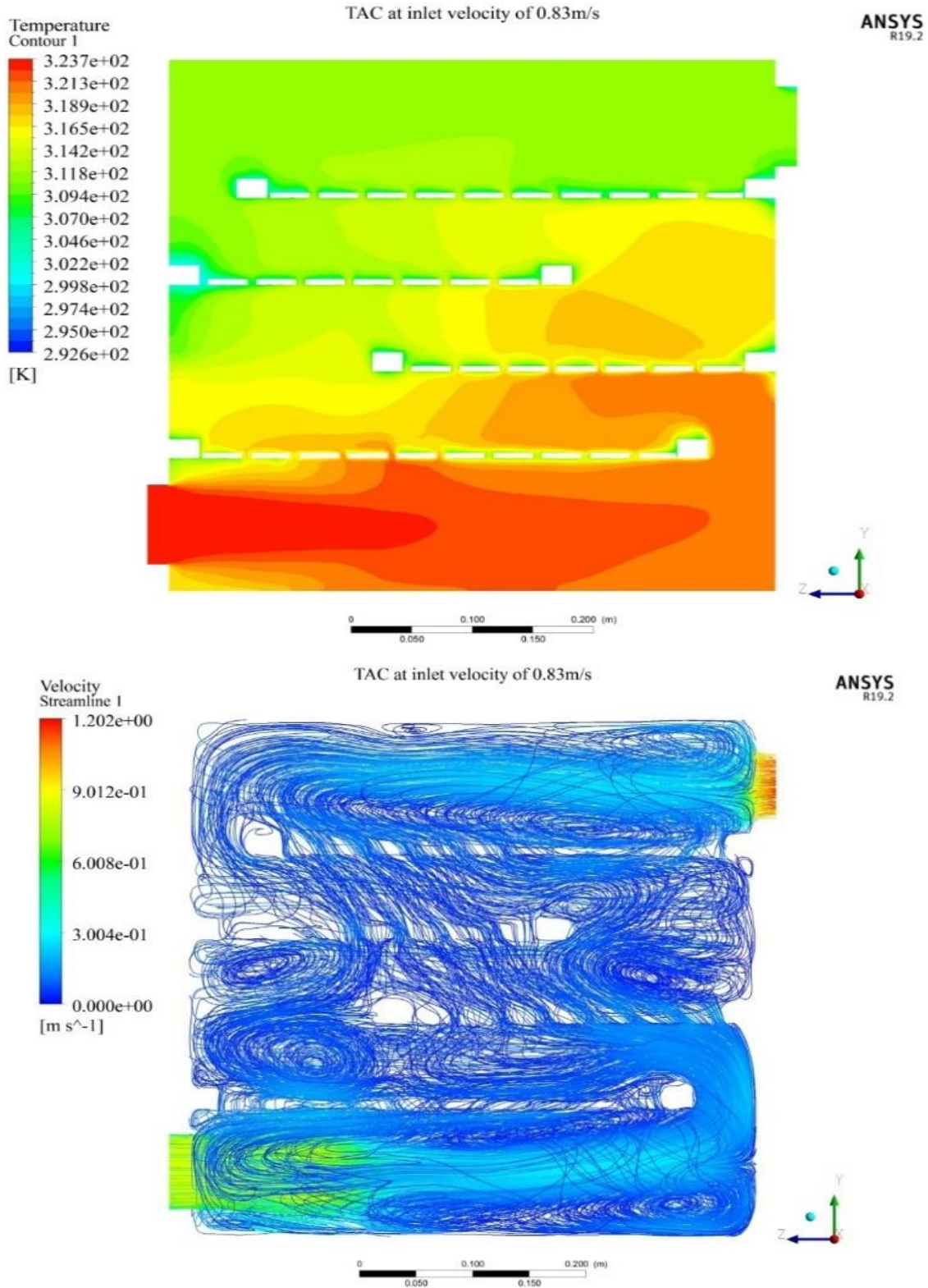
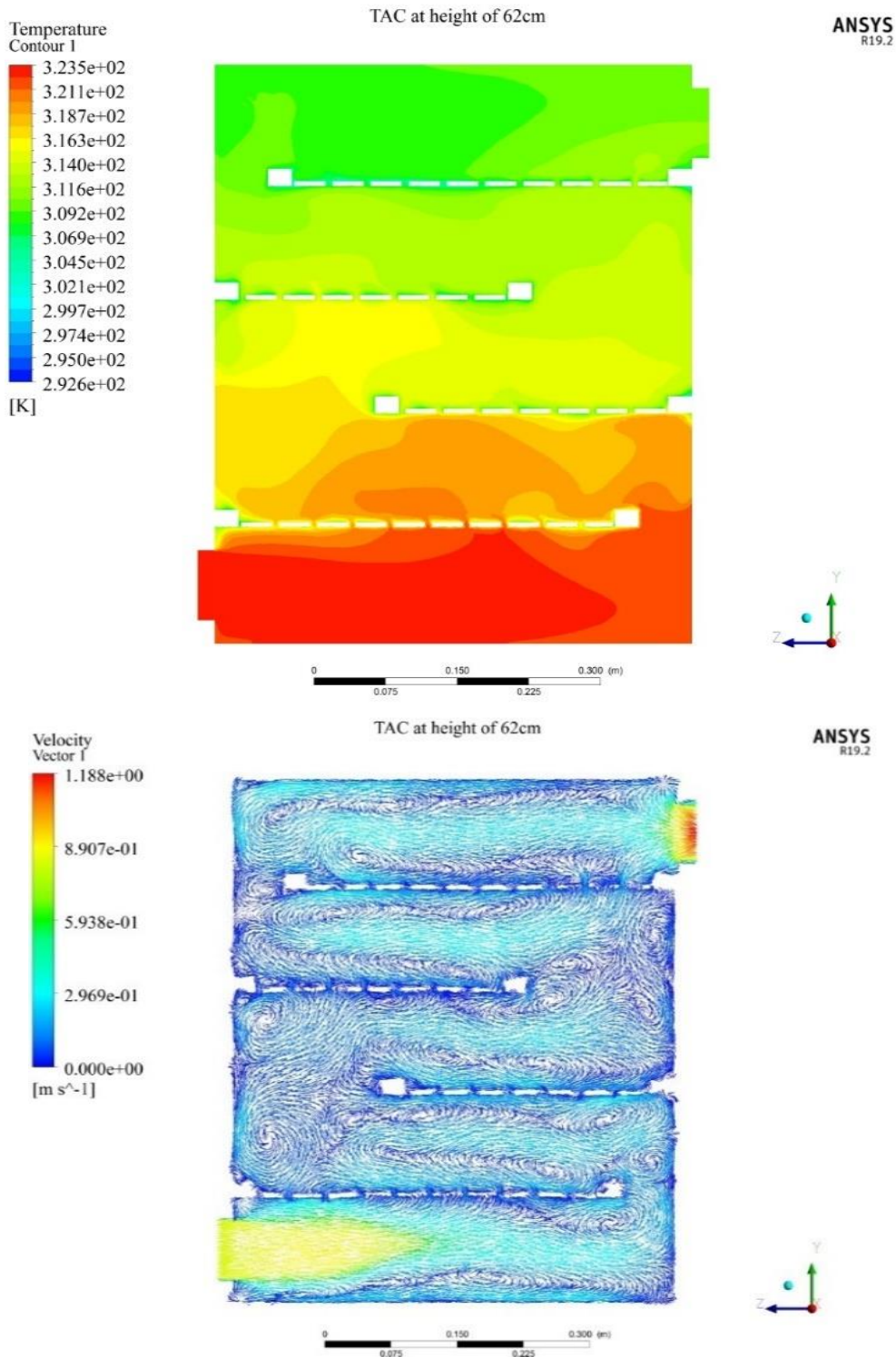


Figure 6: Temperature contour and velocity stream line of the five different tray arrangements

The temperature distributions are non-uniform in all different tray arrangements except the tray arrangement TAC shown in Figure 6. The sample products placed in the bottom tray are at an approximately uniform temperature in TAC rather than in other tray arrangements. Because the trays are not mounted in a zig-zag pattern in TAA, there is no means of direct hot air passage to the next tray, and the flow of hot air is directed directly forward to the outlet of the drying chamber, it creates a heat loss. The first tray gets more heat energy from the drying air, which makes the product dry faster when compared to the second and third trays in TAA. There is no gap that encourages the flow of that hot air to the next tray. The minimum temperature of 292.3K was observed at a maximum temperature of 323.16K in TAA. In TAC, some of the higher temperature drying air flows directly into the second tray via the gap at the end of the right side of the drying chamber, and there is a passage of hot air near the left side of the drying chamber. The flow of the drying hot air is zig-zag, and the trays were placed to act as baffles to disturb the flow of the air. There is a low temperature on the left side of the drying chamber on the third trays in this TAC, but it doesn't cover a large area. In the case of TAB, the expansion of low temperature goes to the sample of banana sliced in half, but in this case, it is near to the end. The temperature flow is more uniform in TAC. In the case of TAC, the direct loss of drying air temperature via the outlet of the drying chamber was minimized. Only two sampled bananas on the bottom tray were exposed to a low temperature compared with the sampled banana on the same tray. This is a good result when compared with TAA, TAB, and TAE. The sample banana in the upper tray is exposed to a uniform drying air temperature. In the case of TAB, the length of the first bottom tray is shorter than the first bottom tray in TAC. Due to this, the hot air tends to start to bend after several paths of flow. The length of the first bottom tray in the case of TAC is shorter compared with the first bottom tray of TAA, and greater than the first bottom tray of TAB. Due to this, there is a direct passage of the hot air to the next tray, passing through the gap between the products. The middle two trays in the case of TAC are shorter than the bottom and upper trays. They are also shorter than the trays in TAB. This makes the flow of the temperature distributions uniform. The minimum temperature of 292.7K was obtained at a maximum temperature of 323.8K on TAD and 323.7K on TAC. This indicates that there are poor temperature distributions in the case of TAD. There was the poorest temperature distribution in the case of TAE since the minimum temperature of 292.6K was obtained at a maximum temperature of 323.8K compared with TAB, TAC, and TAD. As much as possible, the minimum temperature must be increased with an increase in the maximum temperature of the drying chamber. The higher the difference in temperature, the more it indicates there is a poor temperature distribution. Based on the velocity stream line of the five different tray arrangements, there is good air flow in TAA, but it is not uniform after the second tray. The recirculation of the air on the first bottom tray is not as good as TAA in TAB. In TAB, the air tends to move to the second tray through the gap near the right side of the drying chamber. On the uppermost tray, the sampler assumes the product has not had enough contact with drying air. The air flow distribution observed in TAC is a uniform distribution inside

the drying chamber compared to other tray arrangements. The flow velocity is high at the gap of the tray, which is important for mixing of drying temperatures that carry moisture and the drying air that has a greater temperature than the cold air near to the sampled product assumed for drying. From the velocity stream line, it is better to have a higher speed between the tray inside the drying chamber and the drying air, which facilitates the mixing of cold and hot air since there is a temperature difference between the air near the sampled banana and the drying air. From the five different tray arrangements, the minimum maximum air velocity was 1.200m/s in tray arrangement TAE, but the path of the stream line was the poorest, and the next minimum maximum velocity was in tray arrangement TAC, which is 1.202m/s with a good stream line or path. The poor stream line indicates the poor temperature distribution. CFD Simulations of TAC for different heights of the drying chamber Based on the uniformity of temperature and airflow distributions in the symmetry plane, the effect of increasing the height and length of the drying chamber was investigated. Based on the CFD simulation, increasing the height of the drying chamber has better results than increasing the length of the drying chamber. Even when the length of the drying chamber increases, the land required for installing the drying chamber also increases. In the drying chamber at a height of 62 cm, a maximum temperature of 323.5K was observed, with a minimum temperature of 292.6K. In the case of DC 1, the third tray was at a lower temperature, but in the case of DC 2, the temperature contour in the third tray indicates a higher and good temperature contour. With the same TA, the path of the maximum temperature contour in DC 2 is longer, and there is more hot air escaping in the middle of the tray, which is important for drying the product in the second tray. The escaped hot air mixes with the cold air and starts to dry the product. The temperature of the drying air near the sampled product is uniform compared to other DC in DC2. The temperature near the bottom of the drying chamber was uniform and good. In DC 3, the minimum temperature in the case of this drying chamber is 292.6K at a maximum temperature of 323.8K. The path of the warmest temperature is smaller when compared with the height of the drying chamber, which is 62 cm. The flow of the hot air starts to decrease near the inlet of the drying chamber. The upper tray is also not able to get enough temperature. This is due to the loss of heat energy from the hot air due to convective heat transfer on the previous. It is difficult to create a uniform temperature inside the drying chamber; instead, it is better to create a near-to-approximate uniform temperature contour like the drying chamber at a height of 62 cm. The minimum temperature difference between the maximum and minimum temperatures occurred on the DC4 tray arrangement next to the drying chamber at a height of 62 cm.



**Figure 7: Temperature contour for drying chamber with height of 62cm**

The other drawback to increasing the length of the drying chamber is the space requirement of 16.22% more than the space required by the drying chamber with a length of 74 cm, and space of 72% more is required for the drying chamber with a length of 50 cm. According to the available spread area, the proper design of the drying chamber will be selected. If there is insufficient spreading area, it is recommended to use the drying chamber with a 50cm length, width, and height rather than the drying chamber with a length of 62cm. If there is enough area for designing a drying chamber, a drying chamber with a length of 74 cm or 86 cm is preferred.

The effect of increasing the space between the trays or increasing the drying chamber height agrees with or approximates the vertical space used by some researchers such as 11 cm [36], 12 cm [45], 13 cm [46] in forced indirect solar dryer.

**B. Experiment Result**

Temperature and relative humidity were measured in the unloading test at the ambient air,

the outlet of solar air collector one and the inlet of solar air collector two, between the outlet of solar air collector two and

the inlet of the drying chamber, inside the drying chamber, and the outlet of the drying chamber.

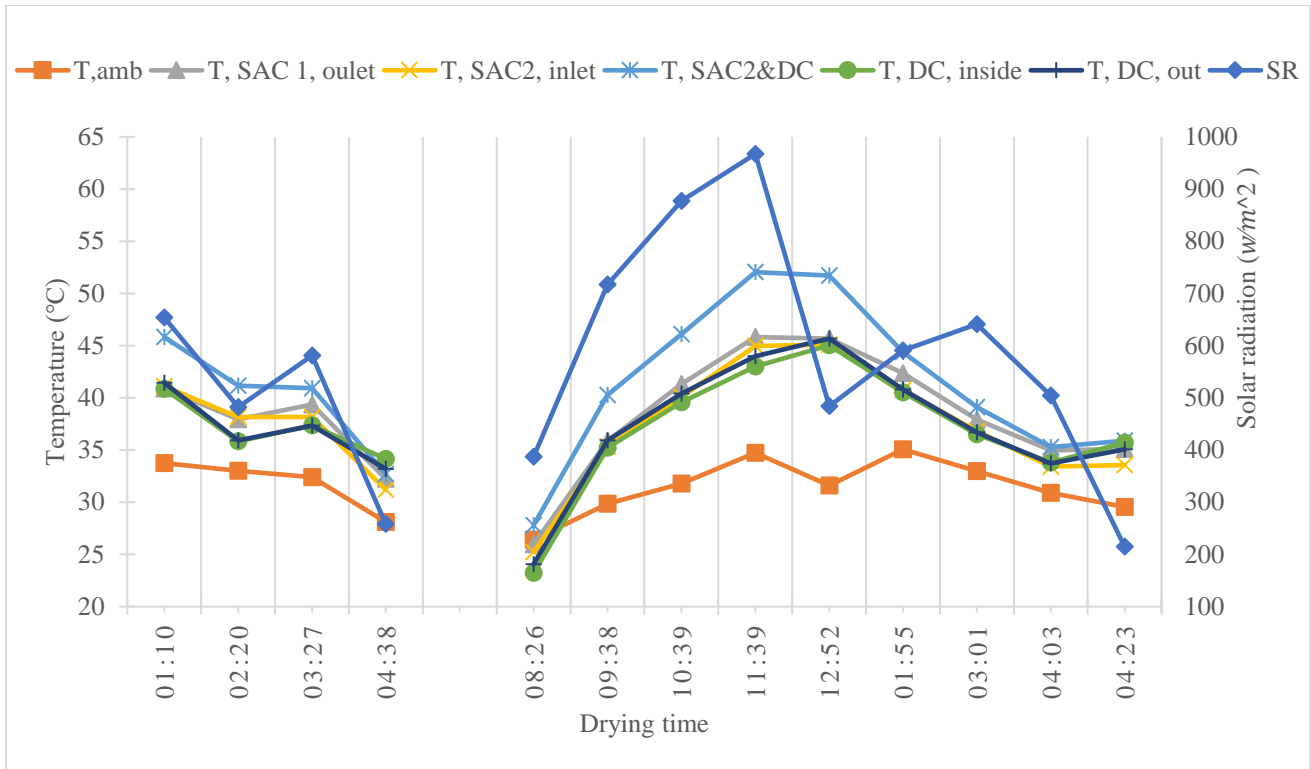


Figure 8: Temperature and solar radiations versus drying time

On the first day of experiment testing of unloading conditions on June 11, 2022, with variations in solar radiation from a minimum of 258.2 to 654.09  $w/m^2$ , the minimum and maximum temperatures of the drying chamber's inlet temperature become 32.71 to 45.84°C, and the minimum and maximum temperatures of the ambient air become 28.11 to 33.76°C, respectively. The average maximum difference between the temperature inside the drying chamber and the outlet of the drying chamber was 0.073°C. The average temperature difference between the outlet of solar air collector one and the inlet of solar air collector two was 0.456°C. These two differences indicate there is no significant loss when the air leaves the solar air collector one and enters into the second solar air collector and there is no loss inside the drying chamber. The temperature inside the drying chamber was greater when the solar radiation became minimum at 4:38 PM due to the air that remained inside the drying chamber. The temperature inside the drying chamber is higher than the ambient air temperature on all days.

On the second day of June 12, 2022, at the time of 8:26AM to 4:23PM, a maximum temperature of 52.04oC at the inlet of the drying chamber was obtained at a maximum solar radiation of 967.4w/m2 at the time of 11:39AM. At the unloading conditions of the experimental test, a maximum average temperature difference of 0.42°C was obtained between the inlet and outlet temperatures of the drying chamber. This indicates that the drying chamber is insulated well. In the full-day experiment test of the solar dryer with unloading conditions, the average temperature between the outlets of the first and second solar air collector was 1.08°C. Throughout the day, the drying chamber's inlet temperature was higher than the ambient temperature. As indicated in all

cases of CFD simulations for temperature distributions, the temperature of the air near to the inlet of the drying chamber is higher. A similar result is obtained here: the inlet temperature of the drying chamber is greater than the inside temperature of the drying chamber. The temperature inside the drying chamber and at the outlet of the drying chamber was approximately equal. The average temperature of the ambient, the outlet of SAC 1, the inlet of SAC 2, the inlet of DC, and the outlet of DC became 31.42°C, 38.74°C, 37.25°C, 41.40, 36.95°C, and 37.37°C, respectively. The outlet of the drying chamber is somehow higher than the inside temperature of the drying chamber, especially at higher solar radiation because the wall of the drying chamber wall painted black absorbs the solar radiation. The solar radiation in the morning, at 8:26AM, was higher than the solar radiation at 4:23PM, but the temperature inside the drying chamber was small. Therefore, it is better to close the inlet of the drying chamber at night and try to heat the solar air collector without running the fan. In the morning at 8:26AM, the outlet and inlet temperatures of the solar air collectors one and two, the inlet of the drying chamber, and the inside temperature of the drying chamber are smaller than the ambient air temperature, so it is better to start the drying after 9:00AM. As the solar intensity increases, so does the temperature.

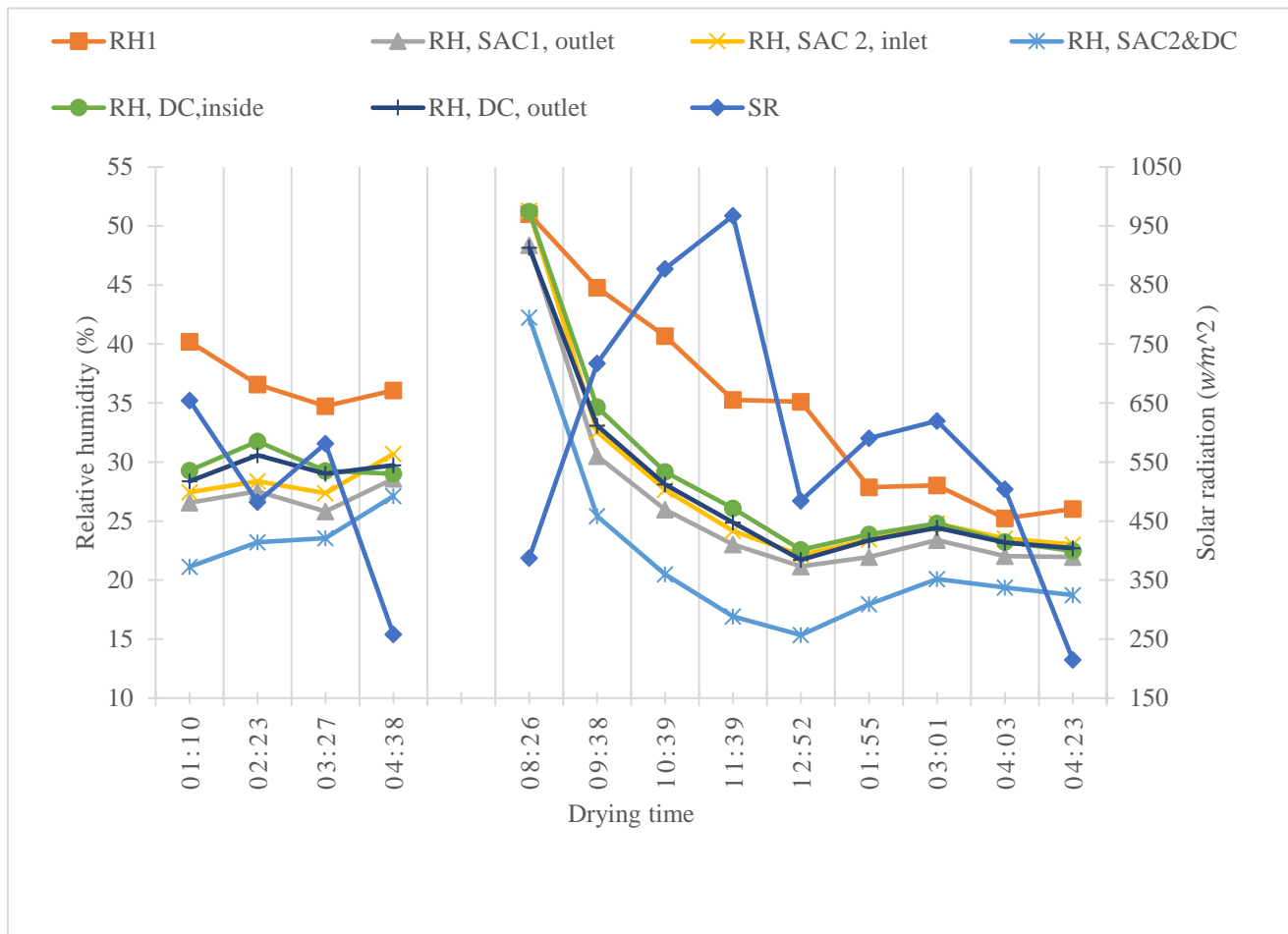


Figure 9: Relative humidity and solar radiations versus time

The Figure 9 shows the relative humidity of the air on June 11, 2022, in the afternoon. From the Figure 9 above, the relative humidity of the air and the solar radiation have an inverse relationship. When solar radiation decreases, the relative humidity of the air increases, and when solar radiation increases, the relative humidity starts to decrease. The relative humidity of the ambient air is higher and the inlet of the drying chamber is lower on all days of the unloading test. The Figure 9 represents the relative humidity of the ambient air, the outlet of SAC 1, the inlet of SAC 2, the inlet of DC, the inside of the DC, and the outlet of DC. The relative humidity at the outlet of SAC 1 and the inlet of SAC 2 was approximately equal, and the relative humidity at the inlet, inside, and outlet of the drying chamber was approximately equal. In the Figure 9, the temperature at the inlet of the drying chamber was the highest, and in reverse, the relative humidity of the air at the inlet of the drying chamber was the lowest. The relative humidity of the air inside the drying chamber and at the outlet of the drying chamber was approximately equal. The relative humidity of the ambient air is the highest of all the days. Due to a small loss in the flexible duct that connects the outlet of the first to the inlet of the second solar air collector, the relative humidity of the air at the inlet of solar air collector two is somehow greater than the relative humidity at the inlet of solar air collector two. As the solar intensity increases, the relative humidity of the air decreases. The data was measured between 1:05 PM and 4:46 PM on June 11, 2022, and between 8:18 AM and 4:28 PM on

June 12, 2022. After the unloading test, the loading test was done. During the loading test, the temperature and relative humidity of the ambient, solar air collector one outlet, solar air collector two inlets, between the outlet of solar air collector two and the inlet of the drying chamber, at each tray and outlet of the drying chamber were measured. The solar radiation was measured at the tilt angle of the solar air collector. On the first day, June 14, 2022, the drying was done between 11:00 PM and 4:30 PM for 5:30 hours. During the loading test, near to the initial time of the drying process, the inside temperature of the drying air was low because of the moisture of the product inside the drying chamber was higher. After 12:43 PM, the solar radiation and temperature start to decrease. The ambient air temperature was higher than the inside temperature of the drying chamber at the start of loading the banana. The temperature difference of the air between the drying chamber's average outlet temperature and the ambient average temperature was 2.12°C. An average temperature difference of 7.91°C was obtained between the inlet and outlet of the drying chamber. The amount of water removed in the designed active solar dryer and open solar dryer was 47.53% and 39.62%, respectively. The inside temperature of the drying chamber is higher than the ambient air temperature on the first day because some of the moisture content was reduced on the first drying day. The moisture removal in the first stage is higher due to the high moisture on the surface of the sample

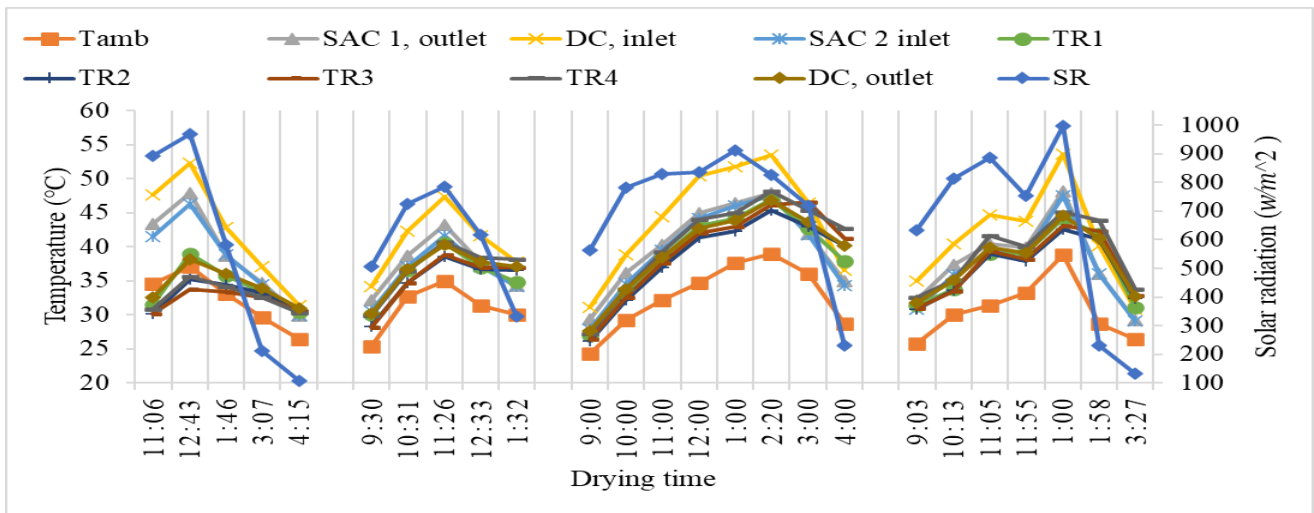


Figure 10: Temperature and Solar intensity versus drying time of four days

Table 9: Unloading test of average solar radiations, temperature and relative humidity

Day		Solar Radiation	Ambient	SAC - 1 outlet	SAC - 2 inlet	SAC - 2 outlet	DC inside	DC outlet
June 11,2022	T (°C)	482.481	31.63	37.35	36.83	39.7	36.81	36.68
	RH (%)		36.66	27.14	28.55	23.96	29.79	29.46
June 12,2022	T (°C)	609.48	31.30	38.21	37.18	41.46	36.76	37.25
	RH (%)		36.37	27.46	29.11	22.64	28.82	28.73

The drying of the product on the second day June 15, 2022 was start from 9:30 AM to 1:30 PM that is for 4hours. The temperature difference between the inlet and outlet let of the drying chamber was 4.26°C that is smaller than the change in temperature in the first drying period, the small difference in temperature indicates the product is in the stage of drying. The difference between the average outlet temperature of the drying chamber and average ambient air temperature was 4.39°C. In this drying day the moisture content removed from the banana in the designed and open sun dyer were 25.80% and 11.97% respectively which is smaller when compared with the first drying period. In the third drying period of June 16, 2022 the maximum average inlet temperature to the drying chamber was 44.32°C while the average ambient air

temperature was 32.77°C at solar radiations of 717.13w/m<sup>2</sup>. The average change in temperature between the inlet and outlet of the drying chamber was 4.66°C and between the average outlet temperature of the air at the outlet of the drying chamber and average temperature of the ambient air was 6.89°C. In the last drying day of June 17, 2022, the average solar radiations of 644.92w/m<sup>2</sup> the average outlet temperature of the solar air collector 41.76°C while the average ambient air temperature was 30.98°C. The change in average temperature of the inlet and outlet of the drying chamber was 3.59°C and the average temperature difference between the outlet of the drying chamber and ambient air temperature 7.19°C which is greatest when compare with all the drying days.

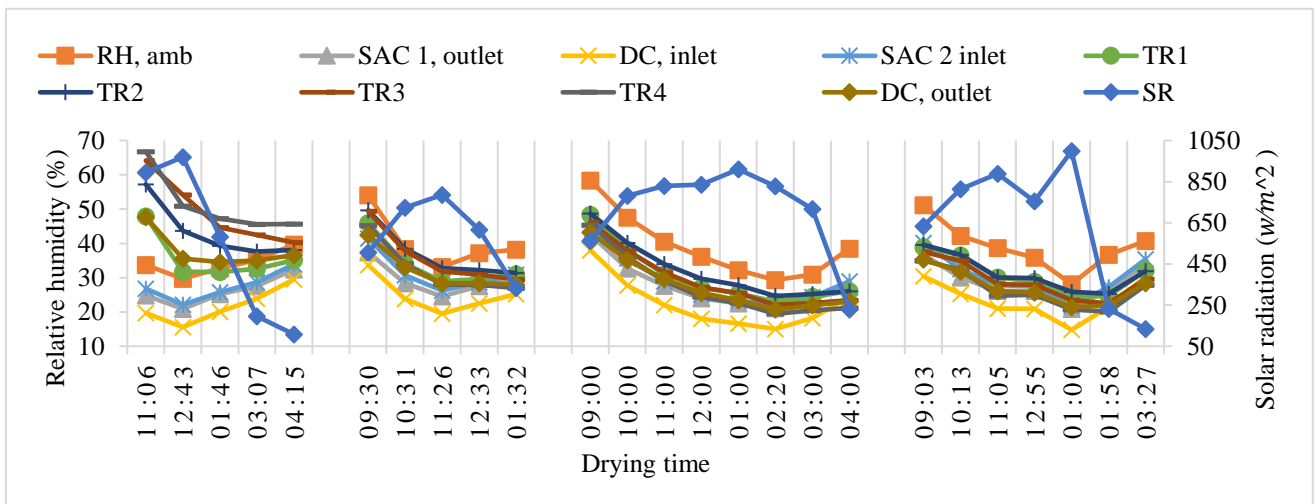


Figure 11: Relative humidity and Solar intensity versus drying time of four days

On the first drying day of June 14, 2022, the average outlet relative humidity of the air at the outlet of the drying chamber was 3.65% greater than the ambient air relative humidity because of the moisture of the banana inside the drying chamber. The average relative humidity of the air is the highest on tray four. Due to the initial moisture content of the banana, the relative humidity of the air increases from tray one to tray four. The relative humidity of the air decreases

with an increase in solar radiation and increases with a decrease in solar radiation. The relative humidity of the air at the outlet of the drying chamber was also higher in the first two hours of drying. On the second drying day of June 15, 2022, the relative humidity of the outlet of the drying chamber was lower than the ambient air relative humidity. This indicates that the product inside the drying chamber is somehow dried.

**Table 10: Loading test of the average solar radiation, temperature and relative humidity.**

Day		Solar Radiation	Ambient	SAC - 1 outlet	SAC - 2 inlet	SAC - 2 outlet	DC inside	DC outlet
June 14,2022	RH (%)	575.98	34.54	26.13	27.40	21.66	45.61	38.47
	T (°C)	575.98	32.13	39.03	38.33	42.44	32.76	34.16
June 15,2022	RH (%)	591.68	40.07	29.41	31.46	24.86	34.50	31.83
	T (°C)	591.68	30.85	37.21	36.18	40.70	37.06	35.24
June 16,2022	RH (%)	717.13	39.20	27.76	29.40	22.50	29.90	27.88
	T (°C)	717.13	32.77	40.32	39.54	44.32	39.45	39.66
June 17,2022	RH (%)	644.92	38.38	28.13	29.76	23	29.02	26.79
	T (°C)	644.92	30.98	38.04	37.29	41.76	37.88	38.17

Hint: June 14,2022 between 10:59 AM and 4:21 PM; June 15,2022 between 9:24 AM and 1:38 PM; June 16,2022 between 8:55 AM and 4:05 PM; June 17,2022 between 9:00AM and 3:32 PM.

**Experimental data and regression data**

Where MR, exp, SD and MR, pred, SD represent experimental and predicted moisture ratios for solar dryers, respectively; and MR, exp, OSP and MR, pred, OSD represent experimental and predicted moisture ratios for open

sun dryers, respectively. The Diffusions approach and Vermal et al. are thin layer mathematical modeling. When compared with the uniformity of drying products of bananas done on four trays with the current tray arrangements, the difference between the maximum moisture removal and minimum moisture removal was 4.47%, which is low when compared with the result obtained on previous study [22,36]. This minimum difference indicates there is a uniform drying in the designed indirect active solar dryer.

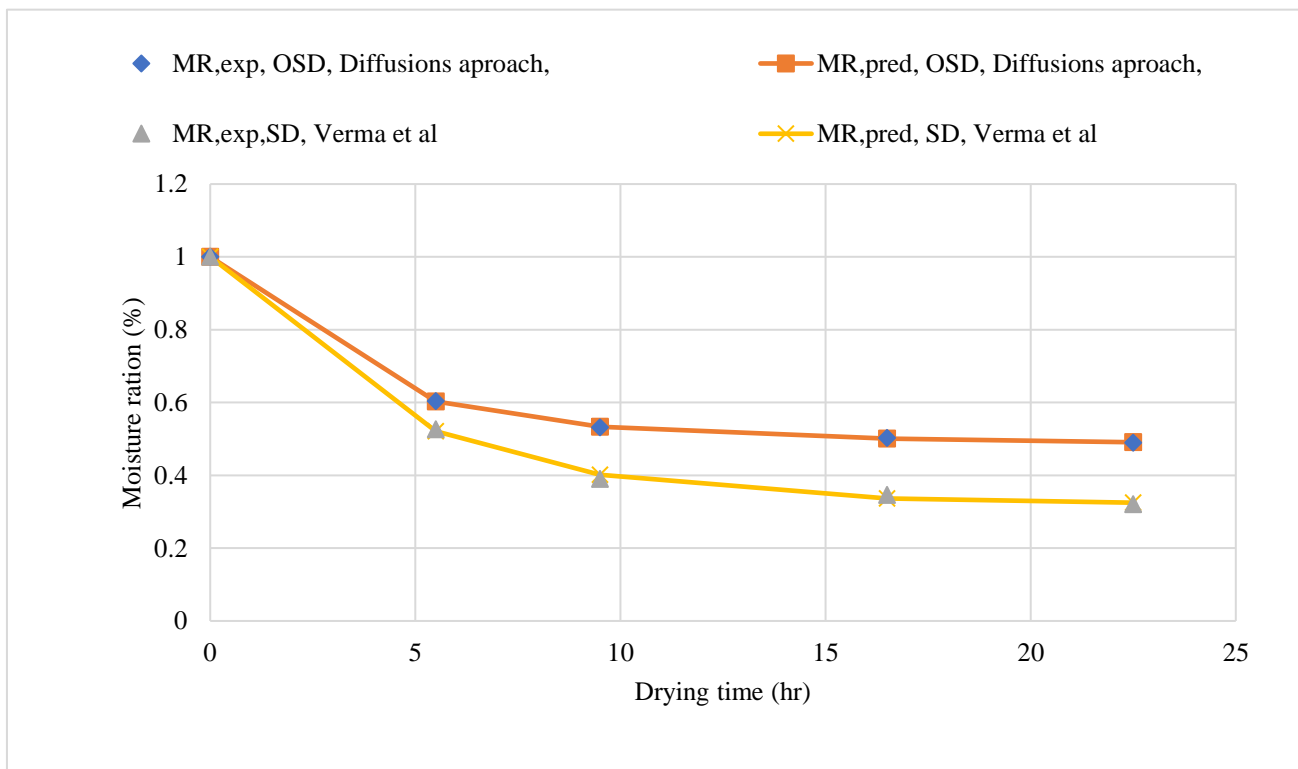


**Figure 12: Experimental data and regression data**

**Table 11: Coefficients of thin layer drying mathematical modeling for open sun dryer**

Modeling	Coefficient	R	X <sup>2</sup>	RMSE
Lewis	$k = 0.0466$	0.879112	0.0155	0.1115
Page	$k = 0.3520, n = 0.2354$	0.998371	0.0002	0.0109
Modified page	$k = 0.0466, n = 1$	0.879112	0.0207	0.1115
Henderson and Pabis	$a = 0.8892, k = 0.0369$	0.864437	0.0157	0.0969
Logarithmic	$a = 0.5067, k = 0.2749, c = 0.4932,$	0.999895	1.9234e-5	0.0028
Two terms	$a = 0.9920, b = 0.2799, k_0 = 0.1151, k_1 = -0.0696$	0.992444	0.0028	0.0235
Wang and Singh	$a = -0.0703, b = 0.0022,$	0.971501	0.0038	0.0480
<b>Verma et al</b>	<b><math>a = 0.5168, k = 0.0023, g = 0.2999</math></b>	<b>0.999974</b>	<b>4.7216e-6</b>	<b>0.0014</b>
Midilli and Kucuk	$a = 1.0001, k = 0.2413, n = 0.5336, b = 0.0094$	0.999729	9.934e-5	0.0045
<b>Diffusion approach</b>	<b><math>a = 0.4832, k = 3000, b = 0.0078</math></b>	<b>0.999974</b>	<b>4.72e-6</b>	<b>0.001374</b>
Two term exponentials	$a = 0.1445, k = 0.2539$	0.918288	0.0129	0.0880
Simplified Fick's diffusion	$a = 0.8892, c = 0.2129, L = 2.4007$	0.864437	0.0235	0.0969
Modified Page equation -2	$k = 0.2934, L = 0.6790, n = 0.2354$	0.998371	0.0003	0.0109
Approximate of diffusions	$a = 1.0033, k = 0.1170, b = 50.4000$	0.992611	0.0015	0.0241

**Table 12: Coefficients of thin layer drying mathematical modeling for designed solar dryer**

Modeling	Coefficient	R	X <sup>2</sup>	RMSE
Lewis	$k = 0.0770$	0.94302	0.0124	0.0998
Page	$k = 0.3559, n = 0.3873$	0.971817	0.0007	0.0209
Modified page	$k = 0.075, n = 1$	0.940984	0.0167	0.1000
Henderson and Pabis	$a = 0.9217, k = 0.0684$	0.93404	0.0144	0.0929
Logarithmic	$a = 0.6812, k = 0.2221, c = 0.3195,$	0.999571	0.000136	0.007376
Two terms	$a = 0.6812, b = 0.3195, k_0 = 0.2221, k_1 = 0$	0.999571	0.0002720	0.007376
Wang and Singh	$a = -0.0880, b = 0.0026,$	0.981968	0.0042	0.0501
<b>Verma et al</b>	<b><math>a = 0.3108, k = -0.0013, g = 0.2181</math></b>	<b>0.999574</b>	<b>0.0001352</b>	<b>0.007353</b>
Midilli and Kucuk	$a = 1.0002, k = 0.2017, n = 0.7838, b = 0.0102$	0.999162	0.0005	0.0103
Diffusion approach	$a = 0.4208, k = 7.0961, b = 0.0703$	0.99368	0.0020	.0283
Two term exponentials	$a = 0.2039, k = 0.2906$	0.964811	0.0094	0.0749
Simplified Fick's diffusion	$a = 0.9217, c = 0.1847, L = 1.6430$	0.93404	0.0216	0.0929
Modified Page equation -2	$k = 0.2414, L = 0.6058, n = 0.3873$	0.996536	0.0011	0.0209
Approximate of diffusions	$a = 1.0079, k = 0.1407, b = 11.8100$	0.998037	0.0007	0.0168

From fourteen different mathematical drying thin layer models, based on the maximum correlation coefficient, minimum root mean square, and minimum reduced chi square, the Verma et al. model and the approximation

diffusion model are respectively the most suitable for active designed solar dryer and open sun dryer for the June experiment.

**Table 13: Performance evaluations**

Performance evaluation	Formula	Indirect active solar dryer	Open sun dryer
Drying rate	$DR = (M_{t+\Delta t} - M_t) / \Delta t$	1.94g/hr	0.37g/hr
Moisture ratio	$MR = M_t / M_i$	0.32	0.49
Moisture removal rate	$MC = (M_i - M_f) \times 100 / M_i$	68.01%	51.01%
Moisture content (dry)	$MC = (M_i - M_f) \times 100 / M_f$	212.64%	104.13%

**V. CONCLUSIONS**

In this study, the design and prototype of the designer active indirect solar dryer were investigated and its performance was compared with the open sun dryer. Computation fluid dynamics was used for the study of the effects of different tray arrangements; the effect of increasing the length and height of the drying chamber. As mentioned in different research [22, 47, 48] the efficiency of the active indirect active solar dryer is higher than the open sun dryer and it is also free from contact with dust, pollution, insects, animals,

microorganisms, and direct solar radiation. Based on the CFD simulation results for the tray arrangement TAC, increasing the height of the drying chamber instead of increasing the length of the drying chamber gives a uniform air temperature and air flow distribution. Recycling the air from the outlet of the drying chamber on the first day is not possible because the quality of the air is lower when compared with ambient air.



The outlet air temperature and relative humidity of the drying chamber are 4.39°C higher and 8.24% less than the ambient air, so it is possible to recycle the air. In the designed indirect active solar dryer and open sun dryer, the moisture removal was 68.01% and 51.01%, respectively, in the drying time of 22.5 hours. That is, the moisture removal rate of the designed indirect active solar dryer is 17% more than the open sun dryer. The average air temperature at the outlet of the solar air collector two was found to be about 9.8°C to 11.41°C higher than the average ambient air temperature, and the outlet relative humidity of the air at the second solar air collector was in the range of 12% to 16.7% below the average ambient air temperature for an average solar radiation of between 493.9 w/m<sup>2</sup> and 711.58w/m<sup>2</sup>.

From the 14 drying kinetic mathematical models with a maximum correlation coefficient of 0.999574 and with a minimum root mean square of 0.0001352 and a minimum reduced chi-square of 0.007353, Verma et al. better fit the experimental results. In a four-day sunlight drying test with a total of 22.5 drying hours in the same climatic conditions, there was a removal of 70.30%, 65.83%, and 51.01% from the upper tray, lower tray, and open sun dryer, respectively. When compared with the uniformity of drying products of banana done on four trays with the current tray arrangement, the difference between the maximum moisture removal and minimum moisture removal was 4.47%, which is low when compared with the results obtained in previous studies [22, 36, 49]. This minimum difference indicates there is a uniform drying in the designed indirect active solar dryer.

**DECLARATION**

Funding/ Grants/ Financial Support	No, I did not receive any financial support for this article.
Conflicts of Interest/ Competing Interests	No conflicts of interest to the best of our knowledge.
Ethical Approval and Consent to Participate	No, this article does not require ethical approval and consent to participate with evidence.
Availability of Data and Material/ Data Access Statement	Not relevant.
Authors Contributions	All authors having equal contribution for this article.

**REFERENCE**

1. V. Belessiotis and E. Delyannis, "Solar drying," Sol. Energy, vol. 85, no. 8, pp. 1665–1691, 2011, doi: 10.1016/j.solener.2009.10.001. [CrossRef]
2. A. Tiwari, "A Review on Solar Drying of Agricultural Produce," Food Process. Technol., vol. 7, no. 9, 2016, doi: 10.4172/2157-7110.1000623. [CrossRef]
3. V. P. Chandramohan, "Experimental Analysis and Simultaneous Heat and Moisture Transfer with Coupled CFD Model for Convective Drying of Moist Object," Int. J. Comput. Methods Eng. Sci. Mech., vol. 17, no. 1, pp. 59–71, 2016, doi: 10.1080/15502287.2016.1147506. [CrossRef]
4. A. Sharma, C. R. Chen, and N. Vu Lan, "Solar-energy drying systems: A review," Renew. Sustain. Energy Rev., vol. 13, no. 6–7, pp. 1185–1210, 2009, doi: 10.1016/j.rser.2008.08.015. [CrossRef]
5. P. Raturi, V. Panwar, and S. Singh, "Characterization of banana peel ionic polymer membrane by using polynomial regression," Mater.

Today Proc., no. xxxx, pp. 1–3, 2021, doi: 10.1016/j.matpr.2021.01.719. [CrossRef]

6. V. N. Hegde, V. S. Hosur, S. K. Rathod, P. A. Harsoor, and K. B. Narayana, "Design, fabrication and performance evaluation of solar dryer for banana," Energy. Sustain. Soc., 2015, doi: 10.1186/s13705-015-0052-x. [CrossRef]
7. E. Getahun, M. A. Delele, N. Gabbiye, S. W. Fanta, P. Demissie, and M. Vanierschot, "Importance of integrated CFD and product quality modeling of solar dryers for fruits and vegetables: A review," Sol. Energy, vol. 220, no. March, pp. 88–110, 2021, doi: 10.1016/j.solener.2021.03.049. [CrossRef]
8. S. Tiwari and G. N. Tiwari, "Energy and exergy analysis of a mixed-mode greenhouse-type solar dryer, integrated with partially covered N-PVT air collector," Energy, vol. 128, no. 2017, pp. 183–195, 2017, doi: 10.1016/j.energy.2017.04.022. [CrossRef]
9. Y. M. Yunus and H. H. Al-Kayiem, "Simulation of Hybrid Solar Dryer Simulation of Hybrid Solar Dryer," 2013 IOP Conf. Ser. Earth Env., 2013, doi: 10.1088/1755-1315/16/1/012143. [CrossRef]
10. A. Mellalou, W. Riad, S. K. Hnawi, A. Tchenka, A. Bacaoui, and A. Outzourhit, "Experimental and CFD Investigation of a Modified Uneven-Span Greenhouse Solar Dryer in No-Load Conditions under Natural Convection Mode," Int. J. Photoenergy, vol. 2021, 2021, doi: https://doi.org/10.1155/2021/9918166 Research. [CrossRef]
11. M. Iranmanesh, H. Samimi Akhijahani, and M. S. Barghi Jahromi, "CFD modeling and evaluation the performance of a solar cabinet dryer equipped with evacuated tube solar collector and thermal storage system," Renew. Energy, vol. 145, no. 2020, pp. 1192–1213, 2019, doi: 10.1016/j.renene.2019.06.038. [CrossRef]
12. Y. Amanlou and A. Zomorodian, "Applying CFD for designing a new fruit cabinet dryer," J. Food Eng., vol. 101, no. 1, pp. 8–15, 2010, doi: 10.1016/j.jfoodeng.2010.06.001. [CrossRef]
13. M. Vivekanandan, K. Periasamy, C. D. Babu, G. Selvakumar, and R. Arivazhagan, "Experimental and CFD investigation of six shapes of solar greenhouse dryer in no load conditions to identify the ideal shape of dryer," Mater. Today Proc., vol. 37, no. Part 2, pp. 1409–1416, 2020, doi: 10.1016/j.matpr.2020.07.062. [CrossRef]
14. O. Prakash, V. Laguri, A. Pandey, A. Kumar, and A. Kumar, "Review on various modelling techniques for the solar dryers," Renew. Sustain. Energy Rev., vol. 62, pp. 396–417, 2016, doi: 10.1016/j.rser.2016.04.028. [CrossRef]
15. A. K. Babu, G. Kumaresan, V. Antony Aroul Raj, and R. Velraj, "CFD studies on different configurations of drying chamber for thin-layer drying of leaves," Energy Sources, Part A Recover. Util. Environ. Eff., vol. 42, no. 18, pp. 2227–2239, 2020, doi: 10.1080/15567036.2019.1607935. [CrossRef]
16. A. Ghaffari and R. Mehdipour, "Modeling and Improving the Performance of Cabinet Solar Dryer Using Computational Fluid Dynamics," Int. J. Food Eng., vol. 11, no. 2, pp. 157–172, 2015, doi: 10.1515/ijfe-2014-0266. [CrossRef]
17. A. Ghazanfari, L. Tabil, and S. Sokhansanj, "Evaluating a solar dryer for in-shell drying of split pistachio nuts," Dry. Technol., vol. 21, no. 7, pp. 1357–1368, 2003, doi: 10.1081/DRT-120023183. [CrossRef]
18. A. Umayal Sundari, P. Neelamegam, and C. V. Subramanian, "An Experimental Study and Analysis on Solar Drying of Bitter Gourd Using an Evacuated Tube Air Collector in Thanjavur, Tamil Nadu, India," Conf. Pap. Energy, vol. 2013, pp. 1–4, 2013, doi: 10.1155/2013/125628. [CrossRef]
19. H. Schütz, M. Jansen, and M. A. Verhoff, "Vom alkohol zum liquid ecstasy (GHB) - Ein überblick über alte und moderne K.-o.-Mittel - Teil 3:  $\gamma$ -Hydroxybuttersäure (GHB, 'liquid ecstasy')," Archiv für Kriminologie, vol. 228, no. 5–6, pp. 151–159, 2011.
20. W. Aissa, M. El-Sallak, and A. Elhakem, "Performance of solar dryer chamber used for convective drying of sponge-cotton," Therm. Sci., vol. 18, no. SUPPL.2, pp. 451–462, 2014, doi: 10.2298/TSCI110710084A. [CrossRef]
21. K. R. Arun, M. Srinivas, C. A. Saleel, and S. Jayaraj, "Active drying of unripened bananas (Musa Nendra) in a multi-tray mixed-mode solar cabinet dryer with backup energy storage," Sol. Energy, vol. 188, no. 2019, pp. 1002–1012, 2019, doi: 10.1016/j.solener.2019.07.001. [CrossRef]
22. M. Kumar, S. K. Sansaniwal, and P. Khatkhat, "Progress in solar dryers for drying various commodities," Renew. Sustain. Energy Rev., vol. 55, pp. 346–360, 2016, doi: 10.1016/j.rser.2015.10.158. [CrossRef]



23. P. Mehta, S. Samaddar, P. Patel, B. Markam, and S. Maiti, "Design and performance analysis of a mixed mode tent-type solar dryer for fi sh-drying in coastal areas," *Sol. Energy*, vol. 170, pp. 671–681, 2018, doi: 10.1016/j.solener.2018.05.095. [[CrossRef](#)]
24. I. Farkas, I. Seres, and C. Mészáros, "Analytical and experimental study of a modular solar dryer," *Renew. Energy*, vol. 16, pp. 773–778, 1999, doi: 10.1016/S0960-1481(98)00278-X. [[CrossRef](#)]
25. R. Poblete, E. Cortes, J. Macchiavello, and J. Bakit, "Factors influencing solar drying performance of the red algae *Gracilaria chilensis*," *Renew. Energy*, vol. 126, pp. 978–986, 2018, doi: 10.1016/j.renene.2018.04.042. [[CrossRef](#)]
26. S. Misha, S. Mat, M. H. Ruslan, K. Sopian, and E. Salleh, "The Prediction of Drying Uniformity in Tray Dryer System using CFD Simulation," vol. 3, no. 5, 2013, doi: 10.7763/IJMLC.2013.V3.352. [[CrossRef](#)]
27. S. Anand, D. P. Mishra, and S. K. Sarangi, "CFD supported performance analysis of an innovative biomass dryer," *Renew. Energy*, vol. 159, no. 2020, pp. 860–872, 2020, doi: 10.1016/j.renene.2020.06.039. [[CrossRef](#)]
28. N. Kottayat, S. Kumar, A. K. Yadav, and S. Anish, "Computational and experimental studies on the development of an energy-efficient drier using ribbed triangular duct solar air heater," *Sol. Energy*, vol. 209, no. September, pp. 454–469, 2020, doi: 10.1016/j.solener.2020.09.012. [[CrossRef](#)]
29. F. Erdog̃du, M. Linke, U. Praeger, M. Geyer, and O. Schlüter, "Experimental determination of thermal conductivity and thermal diffusivity of whole green ( unripe ) and yellow ( ripe ) Cavendish bananas under cooling conditions," *J. Food Eng. J.*, vol. 128, pp. 46–52, 2014, doi: 10.1016/j.jfoodeng.2013.12.010. [[CrossRef](#)]
30. E. K. Akpinar and Y. Bicer, "Mathematical modelling of thin layer drying process of long green pepper in solar dryer and under open sun," *Energy Convers. Manag.*, vol. 49, no. 2008, pp. 1367–1375, 2008, doi: 10.1016/j.enconman.2008.01.004. [[CrossRef](#)]
31. I. N. Simate and S. Cherotich, "Design and Testing of a Natural Convection Solar Tunnel Dryer for Mango," *J. Sol. Energy*, vol. 2017, 2017, doi: 10.1155/2017/4525141 Research. [[CrossRef](#)]
32. J. P. Ekka, K. Bala, P. Muthukumar, and D. K. Kanaujiya, "Performance analysis of a forced convection mixed mode horizontal solar cabinet dryer for drying of black ginger (*Kaempferia parviflora*) using two successive air mass flow rates," *Renewable Energy*, vol. 152, pp. 55–66, 2020, doi: 10.1016/j.renene.2020.01.035. [[CrossRef](#)]
33. Z. Alimohammadi, H. Samimi Akhijahani, and P. Salami, "Thermal analysis of a solar dryer equipped with PTSC and PCM using experimental and numerical methods," *Sol. Energy*, vol. 201, pp. 157–177, 2020, doi: 10.1016/j.solener.2020.02.079. [[CrossRef](#)]
34. A. Khanlari, "Thermal performance improvement of an indirect solar dryer with tube-type absorber packed with aluminum wool," *Sol. Energy*, vol. 217, pp. 328–341, 2021, doi: 10.1016/j.solener.2021.02.029. [[CrossRef](#)]
35. F. Nasri, "Solar thermal drying performance analysis of banana and peach in the region of Gafsa (Tunisia)," *Case Stud. Therm. Eng.*, vol. 22, p. 100771, 2020, doi: 10.1016/j.csite.2020.100771. [[CrossRef](#)]
36. A. Lingayat, V. P. Chandramohan, and V. R. K. Raju, "Design, Development and Performance of Indirect Type Solar Dryer for Banana Drying," *Energy Procedia*, vol. 109, no. 2017, pp. 409–416, 2017, doi: 10.1016/j.egypro.2017.03.041. [[CrossRef](#)]
37. A. Midilli and H. Kucuk, "Mathematical modeling of thin layer drying of pistachio by using solar energy," *Energy Convers. Manag.*, vol. 44, no. 7, pp. 1111–1122, 2003, doi: 10.1016/S0196-8904(02)00099-7. [[CrossRef](#)]
38. T. Gunhan, V. Demir, E. Hancioglu, and A. Hepbasli, "Mathematical modelling of drying of bay leaves," *Energy Convers. Manag.*, vol. 46, pp. 1667–1679, 2005, doi: 10.1016/j.enconman.2004.10.001. [[CrossRef](#)]
39. A. A. El-Sebaei and S. M. Shalaby, "Experimental investigation of an indirect-mode forced convection solar dryer for drying thymus and mint," *Energy Convers. Manag.*, vol. 74, pp. 109–116, 2013, doi: 10.1016/j.enconman.2013.05.006. [[CrossRef](#)]
40. M. Younis, D. Abdelkarim, and A. Zein El-Abdein, "Kinetics and mathematical modeling of infrared thin-layer drying of garlic slices," *Saudi J. Biol. Sci.*, vol. 25, no. 2018, pp. 332–338, 2017, doi: 10.1016/j.sjbs.2017.06.011. [[CrossRef](#)]
41. T. Hadibi, A. Boubekri, and D. Mennouche, "3E analysis and mathematical modelling of garlic drying process in a hybrid solar-electric dryer," *Renew. Energy*, vol. 170, no. 2021, pp. 1052–1069, 2021, doi: 10.1016/j.renene.2021.02.029. [[CrossRef](#)]
42. L. Ait Mohamed, C. S. Ethmane Kane, M. Kouhila, A. Jamali, M. Mahrouz, and N. Kechaou, "Thin layer modelling of *Gelidium sesquipedale* solar drying process," *Energy Convers. Manag.*, vol. 49, no. 5, pp. 940–946, 2008, doi: 10.1016/j.enconman.2007.10.023. [[CrossRef](#)]
43. S. Mghazli, M. Ouhammou, N. Hidar, L. Lahnine, A. Idlimam, and M. Mahrouz, "Drying characteristics and kinetics solar drying of Moroccan rosemary leaves," *Renew. Energy*, vol. 108, no. 2017, pp. 303–310, 2017, doi: 10.1016/j.renene.2017.02.022. [[CrossRef](#)]
44. B. Yelmen, Ç. Ün, H. Hande, and M. Yüksekdağ, "Mathematical modelling of greenhouse drying of red chilli pepper," *African J. Agric. Res. Full*, vol. 14, no. 9, pp. 539–547, 2019, doi: 10.5897/AJAR2018.13748. [[CrossRef](#)]
45. M. A. Hossain, B. M. A. Amer, and K. Gottschalk, "Hybrid solar dryer for quality dried tomato," *Dry. Technol.*, vol. 26, no. 12, pp. 1591–1601, 2008, doi: 10.1080/07373930802467466. [[CrossRef](#)]
46. N. A. Vlachos, T. D. Karapantsios, A. I. Balouktsis, and D. Chassapis, "DESIGN AND TESTING OF A NEW SOLAR TRAY DRYER," *Dry. Technol. An Int. J.*, vol. 20, no. 6, pp. 1243–1271, 2002, doi: http://dx.doi.org/10.1081/DRT-120004050. [[CrossRef](#)]
47. H. Moussaoui, Y. Bahammou, Z. Tagnamas, M. Kouhila, A. Lamharrar, and A. Idlimam, "Application of solar drying on the apple peels using an indirect hybrid solar-electrical forced convection dryer," *Renew. Energy*, vol. 168, pp. 131–140, 2021, doi: 10.1016/j.renene.2020.12.046. [[CrossRef](#)]
48. T. Nadu, "THIN LAYER DRYING CHARACTERISTICS OF CURRY LEAVES ( MURRAYA KOENIGII )," vol. 21, pp. 359–367, 2017. [[CrossRef](#)]
49. B. Basumatary et al., "Design, Construction and Calibration of Low Cost Solar Cabinet Dryer," *Int. J. Environ. Eng. Manag.*, vol. 4, no. 4, pp. 351–358, 2013.

## AUTHORS PROFILE



**Tigabu Mekonnen Belay (Mr.)** received his BSc and MSc degree in Mechanical (Thermal) Engineering from Addis Ababa Science and Technology University in 2021 and 2022 respectively. He is fast learner, very organized, hard worker, self-start, able to work as individual and team, very interested in successful result, intuitive, and creative. His research interest areas are in solar thermal energy, CFD Simulation, Refrigeration and Air Conditioning, Renewable energy, Energy audit, Design CFD simulation and experimental investigation of solar dryer, and cooling system. He participated in different innovative competition in national and international competitions and become top 50 and 30 finalists at Africa innovation week and Green Innovation Lab program at Reach for Change Ethiopia and won \$1000 and 70000ETB in 2019 and 2022.



**Samson Mekbib Atnaw (PhD)** is currently serving as an associate professor in the department of Mechanical Engineering of Addis Ababa Science and Technology University, Ethiopia. He received his PhD degree in Mechanical Engineering from University Teknologi PETRONAS, Malaysia in 2013. He received his BSc. and MSc. degrees in Mechanical Engineering from Addis Ababa University, Ethiopia in 2004 and 2008 respectively. His research area energy systems, renewable energy technology and fuels. He has more than 70 publications in reputable journals and conferences and thousands of citations and a member of Ethiopian Society of Mechanical Engineers.

**Disclaimer/Publisher's Note:** The statements, opinions and data contained in all publications are solely those of the individual author(s) and contributor(s) and not of the Lattice Science Publication (LSP)/ journal and/or the editor(s). The Lattice Science Publication (LSP) and/or the editor(s) disclaim responsibility for any injury to people or property resulting from any ideas, methods, instructions or products referred to in the content.